Going beyond 20 μm-sized channels for studying red blood cell phase separation in microfluidic bifurcations

Sophie Roman,[1,2,a)] Adlan Merlo,[2,1] Paul Duru,[1,2] Frédéric Risso,[2,1] and Sylvie Lorthois[2,1,b)]
[1]*Université de Toulouse, INPT, UPS, IMFT (Institut de Mécanique des Fluides de Toulouse), Allée Camille Soula, F-31400 Toulouse, France*
[2]*CNRS, IMFT, F-31400 Toulouse, France*

(Received 21 December 2015; accepted 27 April 2016; published online 12 May 2016)

Despite the development of microfluidics, experimental challenges are considerable for achieving a quantitative study of phase separation, i.e., the non-proportional distribution of Red Blood Cells (RBCs) and suspending fluid, in microfluidic bifurcations with channels smaller than 20 μm. Yet, a basic understanding of phase separation in such small vessels is needed for understanding the coupling between microvascular network architecture and dynamics at larger scale. Here, we present the experimental methodologies and measurement techniques developed for that purpose for RBC concentrations (tube hematocrits) ranging between 2% and 20%. The maximal RBC velocity profile is directly measured by a temporal cross-correlation technique which enables to capture the RBC slip velocity at walls with high resolution, highlighting two different regimes (flat and more blunted ones) as a function of RBC confinement. The tube hematocrit is independently measured by a photometric technique. The RBC and suspending fluid flow rates are then deduced assuming the velocity profile of a Newtonian fluid with no slip at walls for the latter. The accuracy of this combination of techniques is demonstrated by comparison with reference measurements and verification of RBC and suspending fluid mass conservation at individual bifurcations. The present methodologies are much more accurate, with less than 15% relative errors, than the ones used in previous *in vivo* experiments. Their potential for studying steady state phase separation is demonstrated, highlighting an unexpected decrease of phase separation with increasing hematocrit in symmetrical, but not asymmetrical, bifurcations and providing new reference data in regimes where *in vitro* results were previously lacking.

I. INTRODUCTION

Oxygen and nutrient delivery to living tissues as well as removal of metabolic waste are essentially determined by the dynamics of blood flow in microvascular networks. These networks are highly heterogeneous, with large distributions in architectural, topological, and hemodynamic properties. Microvascular networks typically involve vessels of diameters spanning from about 4 μm to 100 μm. This represents half to ten times the characteristic size of single red blood cells (RBCs), i.e., a very large range in RBC confinement. Moreover, they exhibit huge spatial and temporal variations in RBC concentration, with some vessels containing no blood cells and some others containing almost no suspending plasma.[9,36,50]

At the scale of microvascular networks, the comprehension of the basic mechanisms underlying the emergence of this tremendous heterogeneity is still largely incomplete. They likely involve a strong coupling between network architecture and blood flow dynamics. Moreover, its

physiological role is still largely unknown. Despite it, or perhaps *thanks to* it, microvascular networks are able to ensure adequate blood supply, feeding every cell in peripheral tissues under a wide range of physiologic conditions and varying metabolic needs. They are also able to adjust to various pathological conditions, including sudden obstructions of vessels or progressive reduction of total microvascular density, often postponing irreversible damage.

At smaller scale (single vessel or bifurcation), because of the large range of RBC concentrations and confinements, various RBC flow regimes, from single file RBC flows in narrow capillaries to highly packed RBCs in larger vessels, can be observed or even coexist at a single bifurcation. These various regimes are at the source of highly non-linear complex rheological behaviors:[34,35] paradoxical reduction of apparent viscosity in vessels with diameter below 300 μm (Fåhræus-Lindquist effect), with a minimum around the RBC characteristic size *in vitro*, which is shifted to higher values *in vivo*; relative reduction of tube hematocrit, i.e., the volume fraction of RBCs in blood within a given vessel, compared with discharge hematocrit, i.e., the volume fraction of RBCs in blood flowing through the same vessel (Fåhræus effect); and non-proportional distribution of RBCs and plasma at diverging microvascular bifurcations, one daughter vessel receiving a higher hematocrit than the feeding vessel, and the other receiving a lower hematocrit (phase separation effect). In microvascular networks, this last effect cumulates at successive bifurcations, inducing a tremendous heterogeneity of the hematocrit among vessels. Thus, the phase separation effect contributes to the above-mentioned coupling between microvascular architecture and dynamics.

In order to understand this coupling and its role in the adjustment of blood supply following normal or pathological architectural changes, large-scale network simulations, where the topology and morphology of the network are either idealized (e.g., square or hexagonal networks) obtained by automatic generation of realistic vascular structures or by segmentation of anatomical datasets, have been performed.[12,13,21–23,27,36,38,41,42] In these works, the complex rheological properties of blood flow in microcirculation, especially the phase separation effect, are either described by empirical laws obtained by least-square adjustment to experimental results (e.g., Refs. 21 and 36), theoretically derived assuming a given RBC flow regime (e.g., single file RBC flows in narrow capillaries[27]), or modeled in an *ad hoc* fashion.[12] From several of these studies, it can be deduced that the chosen phase separation law has a huge influence on the hematocrit distribution in the network, and possibly, on the coupling between architecture and dynamics. For example, in simple idealized square capillary networks, Obrist *et al.*[27] show that their theoretical bifurcation law induces a strong correlation between low flow areas in the network (the occurrence of which is a direct consequence of network topology, see Equation (4.10) and Figure 6 in their paper) and high hematocrit areas. As pointed out by the authors, this "build-up in the corner of [their] generic network" is "unphysiological." On the other hand, Gould and Linninger[12] show that the most widely used empirical formulation of the phase separation effect[33,37] results in too many vessels containing no RBCs compared with available experimental datasets. As pointed out by these authors, "the frequency of RBC-devoid vessels [...] directly depends on the level of a model-specific cutoff parameter, X_0. This parameter determines the minimum volumetric bulk flow of a daughter branch to receive any RBC flux." This strongly suggests a correlation between low flow and low hematocrit vessels. Thus, Gould and Linninger[12] introduce a new *ad hoc* description of the phase separation law, while recognizing that further improvements, namely, assessing the variations of the introduced parameters with the diameters of bifurcation "would require more data sets containing microvascular bifurcations with exact measurements of branch diameters and discharge hematocrit [but that] such data sets are unavailable at this time."

Such a lack of experimental data might seem surprising with regard to the large number of previous *in vitro* and *in vivo* experimental work devoted to the study of the phase separation effect.[2,8,10,15,37,45–47] On one hand, despite the development of microfluidics in the last decade, *in vitro* experiments have not yet permitted to explore phase separation in bifurcations with branches of characteristic size smaller than 20 μm nor in asymmetric channels with at least one branch smaller (both in depth and width) than the other ones. In addition, "room-sized" experimental models, designed according to the principles of kinematic and dynamic similarity,

cannot reproduce the complex rheological properties of RBCs. On the other hand, careful quantitative *in vivo* experiments have demonstrated that the phase separation effect is very limited at diameters above 35 μm and decreases with increasing inlet hematocrit.[37] They have allowed the definition of the following relevant parameters for the description of the phase separation effect:[37] feeding vessel to RBC size ratio, daughter vessels to feeding vessel size ratios, fractions of blood flow of the feeding vessel being diverted into both daughter branches, and inlet discharge hematocrit. An empirical description of phase separation as a function of these parameters has also been obtained.[37] However, the accuracy and robustness of the measurement methods used, while the most advanced at that time, remain to be demonstrated.[6] This might explain why two different versions of this empirical description have been proposed, the last one being "adapted from the original experimental data in order to render predictions more robust for extreme combinations of input hematocrit and diameter distribution."[33] However, the ranges of validity of these empirical laws have not been indicated; all results are being presented as functions of ratios between variables rather than as functions of the measured quantities. Moreover, because of the difficulty of flow control inherent to *in vivo* microvascular experiments, where physiological compensatory responses take place, it is not clear whether the results obtained are valid to describe steady-state situations.[12] Altogether, this sheds doubts on the robustness and accuracy of the only available empirical phase separation law. In this context, because of the difficulty in control and metrology of *in vivo* microvascular experiments (i.e., simultaneous measurement and control of all the relevant variables without inducing compensatory microvascular responses), the current trend is to perform well-controlled fluid mechanics *in vitro* experiments. This should ultimately allow a better understanding of the physics at play and a parametrical characterization of the phase-separation effect in steady state, potentially improving the phenomenological description of Pries *et al*.[33,37]

The aim of the present paper is to present the experimental methodologies and measurement techniques developed for that purpose, especially in the case of channels of capillary size or slightly larger (typically below 20 μm), including asymmetric bifurcations, in the full physiological hematocrit range. The main originalities of the experiment are the following: first, we design polydimethylsiloxane (PDMS) micro-bifurcations made of square channels with different sizes, while most of the recent previous studies used bifurcations made of rectangular channels with unique depth,[15,45,47] which are easier to fabricate;[48] second, we are interested in regimes which are seldom studied (moderately to highly concentrated RBC suspension flows in small micro-channels), while in most previous studies, channels with sizes superior or equal to 20 μm have been used;[2,8,10,15,45–47] and third, we simultaneously aim at a rigorous control of the experimental conditions, including the possibility of varying independently the inlet hematocrit and the flow rate ratio between both daughter branches, and at an *in situ* quantitative measurement of the flow parameters. This is extremely challenging in the considered flow regimes and necessitates a combination of various metrologies, including the comparison with reference measurements, in order to validate the results.

Therefore, in the remainder of this Introduction, the metrological challenges and current possibilities will be presented. Ideally, measuring independently and simultaneously the plasma and RBC velocity profiles and the local RBC volume fraction is needed in order to deduce both blood and RBC flows in each branch of a bifurcation by integration. In the last 20 years, micro-Particle Imaging Velocimetry (μ-PIV) has emerged as a powerful technique to achieve measurements of velocity profiles in rectangular channels or capillary tubes with sub-millimetric characteristic size. A vast amount of studies were devoted to adapt this technique to the characterization of blood flow in microsystems (typically, straight micro-channel of rectangular cross-section), i.e., the measurement of both plasma and RBC velocity fields. Such an application requires to tackle numerous challenges (fluorescent tagging of some RBCs at high hematocrit, correction for the finite optical depth of correlation, etc.) which are summed up in recent papers on that particular topic (see, e.g., Refs. 4, 16, and 31).

However, μ-PIV leads to higher relative errors on the velocity measured near the channel walls where the velocities are smaller. Also, the finite size of the interrogation windows used in

the image correlation algorithm prevents any measurement at a distance from the wall less than half the interrogation windows size. Moreover, close to the wall, image quality can be impaired by diffraction. For these reasons, μ-PIV can be expected to be particularly challenging for small channel sizes for which the phase separation effect is expected to occur. Measurements close to the wall are also critical when one rather wants to study RBC slip and local difference in plasma and RBC velocities in order to derive a rheology model, which has not yet been achieved in these regimes. A practical consequence is that no theoretical reference RBC velocity profile is available to assess the accuracy and robustness of the measurements, which are then often compared with the profiles of Newtonian fluids despite very large differences.[1,19,30] Measuring the suspending fluid velocity field in a simultaneous way of course increases the technical sophistication of the PIV setup. To our knowledge, simultaneous measurements of RBC and plasma flows have thus been limited to low hematocrit values (up to 10%) in large channels ($310 \times 200\,\mu m^2$).[16] Also, for small channel sizes, optical sectioning of the channel depth becomes difficult, and the velocity profile can be measured in only one direction: assumptions have to be made to obtain the full velocity field in the channel cross section that is needed to obtain flow rate by integration.

In order to go beyond these difficulties, we have recently revisited a classical temporal correlation technique and shown how it allows to measure the RBCs maximal velocity at any position along the transverse location in a microchannel, lifting some of the constraint imposed by PIV, namely, the difficulties in obtaining reliable measurements close to the wall.[39] This technique will be used in the present paper, and reasonable assumptions will be made to deduce the full RBC velocity field in the channel cross section, as well as the plasma velocity field.

The hematocrit is usually obtained using a photometric method, based on the measurement of the attenuation of a light beam directed through the blood-filled microchannel. The theoretical framework of such an experimental technique—and its consequences as far as the measurement should be technically performed—has been detailed in a seminal paper by Pries *et al*.[32] In practice, an empirical calibration law is often used, relating the light attenuation measured for different test hematocrit values imposed in the microchannel. If a CCD camera is used to measure attenuation, one can obtain hematocrit profiles along the microchannel transverse direction, averaged over the light path, i.e., the microchannel depth. Such a photometric technique can therefore be used as a stand-alone technique to characterize the cell-free layer (CFL) close to microchannel walls. It has to be performed along with blood and plasma flow rate measurements when one is interested in phase separation effect.[46]

The remainder of the paper will be organized as follows: first, the Materials and Methods used will be described. The experimental techniques and assumptions required to obtain the hematocrit, the RBC and suspending fluid flow rates in the present microfluidic-based approach will be detailed. In Section II, we will first provide results that support and validate the methodology presented in the present paper, as far as the blood flow characterization is concerned. Then, we will turn to preliminary results on the phase separation effect enabling to investigate the validity of previous phase separation laws. Finally, conclusions will be drawn in Section IV.

II. MATERIALS AND METHODS

In order to assess RBC flow at microbifurcations, a microfluidic system mimicking blood microvessels is used, as well as neutrally buoyant suspensions of human RBCs. In the following, the y-, x-, and z-axes correspond to the directions of the incident light beam and of the transverse and longitudinal axes of the channel, respectively, the flow being in the positive z direction.

A. Experimental setup

1. Microchannels

Each polydimethylsiloxane (PDMS) microchannel network used in the present study includes a unique microbifurcation composed of one inlet and two outlet segments. These inlet

and outlet segments are 8 mm-long, square cross-section microchannels of size $10\,\mu m \times 10\,\mu m$ or $20\,\mu m \times 20\,\mu m$. Larger rectangular distribution and drainage channels (typically $100\,\mu m \times 20\,\mu m$ and $50\,\mu m \times 10\,\mu m$) are placed upstream and downstream the microbifurcation. Four types of microbifurcations are used, with different arrangements of the inlet and outlet channel sizes, see Table I. The technique used to produce these multi-depth micro-bifurcations is the well-known technique of soft lithography,[26] using as many glass-chrome photomasks as the number of desired channel depths. These photomasks are successively used to produce the positive relief of the micro-channels in a multi-layered photoresist (SU8), which is then used as a master in the PDMS molding process. For instance, for a $20\,\mu m \times 20\,\mu m$ microchannel separating into two $10\,\mu m \times 10\,\mu m$ branches, a first photomask reproduces the design of the full microbifurcation and is used to produce its positive relief in a $10\,\mu m$-thick SU8 layer. Then, a $20\,\mu m$-thick photoresist layer is deposited on the wafer (some part of which being already covered by a $10\,\mu m$-thick SU8 layer) and is insulated through a second photomask reproducing the design of the $20\,\mu m \times 20\,\mu m$ channel only. It must be mentioned that this process therefore induces the existence of a "step" at the junction between two microchannels of different depths. More details about the microfabrication process (e.g., on moulding and bonding of the PDMS microsystems) can be found in Roman *et al.*[40]

The actual dimensions of the microchannels are within 10% of the desired ones and checked *a posteriori* by measuring the eight of each positive micro-channel on the SU8 master using a profilometer and the width of each PDMS channel using our own optical system and a calibration probe. The actual values are used in the whole following when needed to deduce integrated quantities, such as blood flow.

2. Fluidics

Small reservoirs (Nordson EFD dispense tips), partially filled with the RBCs suspension or the suspending fluid solution, are connected to the input and output channels. Using lock rings and soft tubing, these reservoirs are directly connected to three different outlets of a pressure controller (MicroFluidics Control System 8C, Fluigent) enabling to adjust their pressures independently and, thus, the flow rates in both daughter branches of the bifurcation. The pressure-driven flow ensures very short response times when the set pressure drop is changed and good stability over long periods, enabling to study steady-state phase separation. The pressure gradient applied between the inlet and outlet of a single branch of a microbifurcation is typically in the range of 0.85–4.5 mbar/mm.

3. RBC suspensions

Blood samples of controlled hematocrit are prepared. Blood ($\sim 50\,\mu l$ samples) is collected from healthy consenting donors by finger-stick and immediately diluted in a phosphate buffered saline (PBS) solution (1.3 mM NaH_2PO_4, 9 mM Na_2HPO_4, 140 mM NaCl, pH 7.4) containing 1.5 mg/ml EDTA (Ethylenediaminetetraacetic acid, Fluka) for anticoagulation. RBCs are washed by successive centrifugation and re-suspension of the pellet in a glucose-albumin-sodium-phosphate (GASP) buffer (PBS containing 5.5 mM glucose and 4% Bovine Serum Albumin (Eurobio)). In order to avoid RBC sedimentation, a suspending fluid having the same density as RBCs (1.09–1.11 g/ml) is prepared. It consists of a mixture of concentrated GASP

TABLE I. Description of the 4 types of microbifurcations used in the present study.

	Inlet channel	Outlet channel 1	Outlet channel 2
A	$10\,\mu m \times 10\,\mu m$	$10\,\mu m \times 10\,\mu m$	$10\,\mu m \times 10\,\mu m$
B	$20\,\mu m \times 20\,\mu m$	$20\,\mu m \times 20\,\mu m$	$20\,\mu m \times 20\,\mu m$
C	$20\,\mu m \times 20\,\mu m$	$10\,\mu m \times 10\,\mu m$	$10\,\mu m \times 10\,\mu m$
D	$20\,\mu m \times 20\,\mu m$	$20\,\mu m \times 20\,\mu m$	$10\,\mu m \times 10\,\mu m$

and Optiprep (Axis Shield), a density gradient fluid. The method to prepare this iso-density solution is detailed by Roman *et al.*[40] Finally, the washed RBC pellet is diluted in this solution at the desired concentration, i.e., with feed hematocrit ranging from 5% to 60% of RBC. This is a large range by comparison with most previous *in vitro* studies, where a unique value of the feed hematocrit has been used, ranging from 10% in Ref. 15 to 40% in Ref. 10. Note that a drastic reduction of the RBC volume fraction is observed when the suspension flows from the reservoir into the microsystem, with the tube hematocrits H_t being finally in the range of 2%–20%. However, when dealing with higher feed hematocrits (>60%), the probability of the channels being plugged by accumulations of RBCs in the convergent part of the injection channel or at the bifurcation tip was too high to perform any experiment.

4. Imaging

The imaging system consists of a Leica DMRXA2 microscope with a $\times 20$ (NA = 0.4) long-working distance objective. Image acquisition is performed with a high-speed digital camera (PCO Dimax). Sequences of images of RBCs flowing through the microchannels are recorded. They are used to measure the RBC velocities by the dual-slit technique and to determine the tube hematocrit, as explained later. The acquisition frequency F varies from 500 to 10 000 frames per second (fps) and the number of images recorded is fixed to 30 000. These parameters are chosen according to Ref. 40 to ensure high-quality dual-slit measurements. Images of RBCs flowing in the four types of microbifurcations are presented in Figure 1. Note that all the RBCs imaged are in focus, whatever their position along the microchannel depth is, as the microchannels depth ($10\,\mu$m or $20\,\mu$m) is always less than the depth of field of the optical setup. The spatial calibration of the images is typically in the range of 3–4 pixels per micrometer.

B. Metrological developments

1. Hematocrit measurements

Two different techniques are used to measure the tube hematocrit H_t, i.e., the ratio of the volume of RBC upon the channel volume, depending on the RBC concentration in the microchannel.

If the RBC suspension is sufficiently diluted, individual RBC can be counted. The hematocrit is then given by

$$H_t = \frac{N \times \mathcal{V}_{RBC}}{\mathcal{V}_{channel}}, \tag{1}$$

with N being the number of RBC, each with a volume $\mathcal{V}_{RBC}$, counted in a segment of the microchannel of volume $\mathcal{V}_{channel}$. The volume of human RBCs is $\mathcal{V}_{RBC} = 92\,\mu\text{m}^3$ on average.[5] This counting method is only applicable for suspensions for which RBC are individually discernible, i.e., $H_t < 10\%$ and $H_t < 13\%$ in $20\,\mu\text{m} \times 20\,\mu\text{m}$ and $10\,\mu\text{m} \times 10\,\mu\text{m}$ microchannels, respectively. Therefore, for suspensions with higher concentrations, a photometric method has been developed to determine H_t.

The photometric technique relies on relating a measure of the optical density in the channel to the tube hematocrit H_t (see also, e.g., Refs. 20, 32, 46, and 47). To that end, ensemble averaging is performed on two stacks of images of a given microchannel: a first one recorded with only the suspending fluid filling the channel and a second one recorded while the RBC suspension is flowing. The light attenuation at any point (x, z) is defined as the ratio of the two averaged images thus obtained, $I_0(x,z)/I(x,z)$. A transverse optical density profile can then be computed by averaging over the longitudinal direction z and taking the logarithm: $OD(x) = \log(\langle I_0(x)/I(x)\rangle_z)$, where the brackets $\langle\rangle_z$ denote averaging over the longitudinal direction.

Figure 2 shows a typical optical density profile $OD(x)$ thus obtained. The observed oscillations of the optical density in the transverse direction x are provoked by light diffraction at both channel walls. These oscillations render impossible the precise measurement of any optical

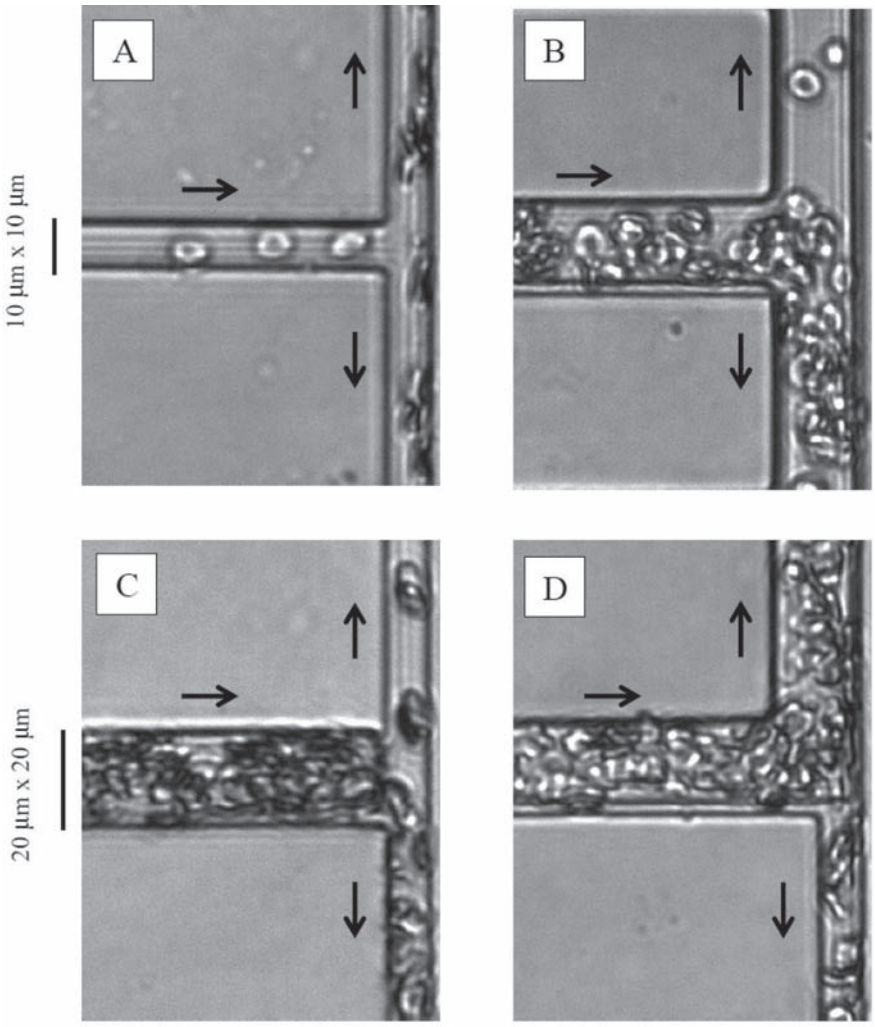

FIG. 1. Typical images of RBC flows in micro-bifurcations. From left to right and top to bottom: microbifurcation of type A, B, C, and D. RBCs are flowing from left to right in the inlet (horizontal) channel. The tube hematocrit in the inlet channel is 3.9%, 5.5%, 13%, and 8%, respectively.

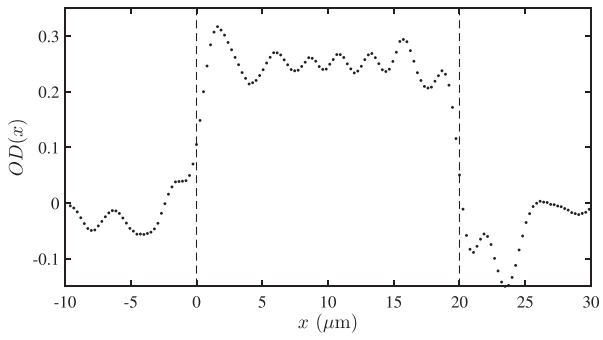

FIG. 2. Typical optical density profile $OD(x)$, obtained from an image sequence of RBC flowing in a 20 μm $\times$ 20 μm microchannel. The vertical dotted lines indicate the location of the microchannel walls.

density gradient close to the channel walls. Note that in larger channels, such oscillations are not present but interpolation of the OD profile must anyway be performed in the vicinity off the walls.[47] Here, one can safely extract from this kind of data a single optical density value, determined as the average of $OD(x)$ for x values in the range of 5–15 μm, i.e., in the center of the channel where OD is observed to be roughly constant. The tube hematocrit H_t is then assumed to be constant over the channel width and related to this mean OD value. To establish the relationship between OD and H_t, the photometric technique is calibrated against the counting technique. In Figure 3, the optical density is shown as a function of H_t determined by counting. For our optical system, the relationship $H_t\,(\text{in}\,\%) = 101.01 \times OD$ is obtained by linear regression (dashed line in Figure 3) within the range of H_t values that can be determined by counting (up to 10%). In the following, we assumed that such a linear relationship between OD and H_t holds up to $H_t = 20\%$ (as observed by Pries *et al.*[32]), and it is used to determine H_t when only OD can be measured. The dominant uncertainty in the use of Equation (1) comes from the counting error, with a relative uncertainty $\delta N/N \approx 15\%$. We estimate the relative uncertainty on the H_t values obtained from optical density measurements to be of the same order of magnitude. Also, the photometric method exposed above is performed sufficiently far upstream the bifurcation in the feeding branch and far downstream the bifurcation in each daughter branch, so that the RBCs have relaxed to a symmetric distribution into the channel. Therefore, the optical density profile is not skewed any more, as seen by Sherwood *et al.* in the close vicinity of bifurcations.[46,47]

Note that for microchannels of section 10 μm $\times$ 10 μm, the photometric method cannot be applied as important intensity oscillations due to light diffraction extend over the full width of the channel. Therefore, the hematocrit is determined by counting, which is possible when $H_t < 13\%$ only. In some cases, however, RBCs flowing in a 10 μm $\times$ 10 μm microchannel are not individually identifiable. In such rare cases, the hematocrit and RBC flow rate may have been determined in the two other channels of the bifurcation (as explained below). Then, the RBC flow rate is first deduced in the channel of unknown hematocrit through the mass conservation principle applied to RBC flow. Finally, knowing the RBC flow rate and the RBC velocity profile measured by dual-slit in the channel of unknown hematocrit, the hematocrit can be calculated.

2. RBC velocity profiles

Velocity profiles of RBCs are measured by the optimized dual-slit technique introduced by Roman *et al.*[40] This temporal correlation technique only converges in steady state conditions. Then, it allows the measurement of a maximal velocity profile, $V_{max}(x)$, that corresponds to the

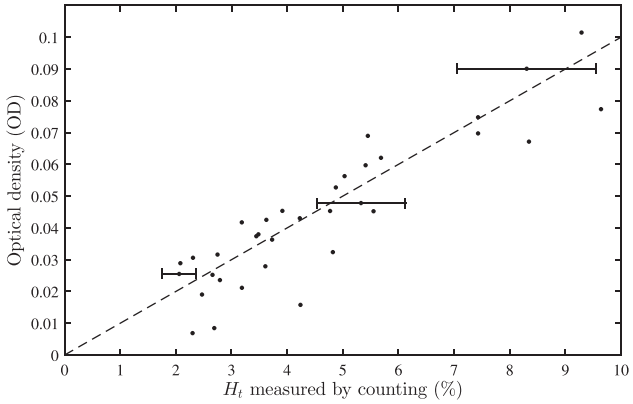

FIG. 3. Optical density as a function of H_t determined by counting, for 20 μm $\times$ 20 μm cross-section channels. Dots: data points; dashed line: best linear fit to the data, $H_t = 101.01 \times OD$. The dominant uncertainty in the use of Equation (1) comes from counting error, with a relative uncertainty $\delta N/N \approx 15\%$. The resulting error-bars on H_t are shown for a few data points only, for the sake of clarity.

RBC velocity profile in the midplane of the microchannel: $V_{max}(x) = V(x, y = 0)$, where $V(x, y)$ is the RBC velocity at any point in the microchannel section.

In Ref. 40, such velocity profiles have been shown to be accurately fitted by the expression

$$V_{max}(x) = V_0\left(1 - B\left(\frac{x}{W/2}\right)^2\right), \tag{2}$$

where W is the width of the channel, $V_0 \equiv V(0,0)$ is the velocity at the center of the channel, and B is a bluntness parameter such as $0 \leq B \leq 1$. If $B = 1$, the velocity profile is parabolic with no slip at walls, whereas if $B = 0$, the profile is flat. Such a description, which was also reported *in vivo* by Pittman and Ellsworth,[29] leads to a slip velocity of RBCs at the channel walls equal to $V_0(1 - B)$.

From the knowledge of $V_{max}(x)$, a full velocity profile for RBCs in the channel cross-section can be obtained by assuming that in all parallel planes of a square cross-section channel, the shape of the velocity profile can be described by Equation (2). Such a velocity profile thus reads

$$V(x,y) = \frac{1}{V_0} \times V_{max}(x) \times V_{max}(y) = V_0 \times \left(1 - B\left(\frac{x}{W/2}\right)^2\right) \times \left(1 - B\left(\frac{y}{W/2}\right)^2\right). \tag{3}$$

3. Determination of RBC and suspending fluid flow rates

The RBC flow rate is obtained by integrating the product of the velocity profile times the tube hematocrit. Assuming that the RBC velocity profile is given by Equation (3), this leads to

$$Q_{RBC} = \int_{-\frac{W}{2}}^{\frac{W}{2}}\int_{-\frac{W}{2}}^{\frac{W}{2}} H_t\, V(x,y)dxdy = H_t \times V_0 \times W^2 \times \left(1 - \frac{1}{3}B\right)^2. \tag{4}$$

Note that for low hematocrits, the number N of RBC flowing through a section of the channel over a period of time Δt can also be determined by visual inspection of the recorded images. The RBC flow rate is then given by

$$Q_{ref,RBC} = \frac{N \times \mathcal{V}_{RBC}}{\Delta t}. \tag{5}$$

Such a way to get the RBC flow rate requires no assumptions to be made about the velocity profile of RBCs and hematocrit variations in the channel cross-section. It provides a reference value for the RBC flow rate, to which data obtained using Equation (4) will be compared below.

Concerning the suspending fluid flow rate, it has been shown for a 100 μm diameter tube and 20% hematocrit that the RBCs and the plasma flow with the same maximal velocity, with a parabolic profile for the plasma.[49] Accordingly, the suspending fluid flow rate is determined in this work by assuming a Newtonian behavior, a maximal suspending fluid velocity equal to the measured maximal RBC velocity and no slip at walls. This assumption will be further discussed in Section III B 3. Under this assumption, the ratio between the maximal velocity of the suspending fluid and its mean velocity is 2.0963 for square channels, as demonstrated by Patzek and Silin.[28] Because the volume fraction of the suspending fluid is equal to $(1 - H_t)$, the suspending fluid flow rate is obtained as

$$Q_f = \frac{V_0}{2.0963} \times W^2 \times (1 - H_t). \tag{6}$$

The total blood flow rate, $Q_{blood} = Q_{RBC} + Q_f$, is straightforwardly determined from Equations (4) and (6). Also, the discharge hematocrit H_d is defined as the ratio between Q_{RBC} and Q_{blood}. Moreover, the fractional blood and RBC flows in daughter branch i of a bifurcation are deduced as $FQ^i_{blood} = Q^i_{blood}/Q^e_{blood}$ and $FQ^i_{RBC} = Q^i_{RBC}/Q^e_{RBC}$, respectively, where subscript e denotes the entry branch.

III. RESULTS AND DISCUSSION

As explained earlier, the measurement of RBC maximal velocity profiles by dual-slit, following Roman *et al.*[40] and described by Equation (2), is at the core of the methodology developed in the present paper. First, we discuss the measured velocity profiles before turning to the validation of the RBC and suspending fluid flow rate measurement techniques proposed in Section II. Finally, preliminary results on phase separation are presented.

A. RBC velocity profiles

For $20\,\mu\text{m} \times 20\,\mu\text{m}$ microchannels, the velocity profile parameters V_0 and B have been determined for 95 different images sequences, with tube hematocrit ranging from 0.7% to 22%. The maximal velocities V_0 varied from 25 to more than $6000\,\mu\text{m/s}$. The parameter B that describes the bluntness of the velocity profile was found to range from 0.04 to 0.66, with mean and standard deviation values equal to 0.25 and 0.12, respectively. No systematic trend for a possible systematic variation of B with H_t nor V_0 could be extracted from this data set. A large dispersion was indeed observed for B values corresponding to similar flow conditions. An example of the rather flat RBC velocity profiles obtained in that case is presented in Figure 4(a). Velocity gradients are clearly visible close to the channel walls, where RBCs are slower than in the center, but with a significant non-zero slip velocity at walls.

For the $10\,\mu\text{m} \times 10\,\mu\text{m}$ case, 55 image sequences were considered with the hematocrit varied from 0.1% to 18%. The maximal velocities V_0 ranged from 7 to more than $1400\,\mu\text{m/s}$. The bluntness parameter B ranged from -0.04 to 0.07, with mean and standard deviation values equal to 0.02 and 0.03, respectively. In that case, maximal velocity profiles are thus flat, see a typical example in Figure 4(b). Note that this remains true even for the largest hematocrit values considered, for which RBCs are no longer organized in single file and nonetheless all move at the same velocity. As before, no systematic trend for a possible systematic variation of B

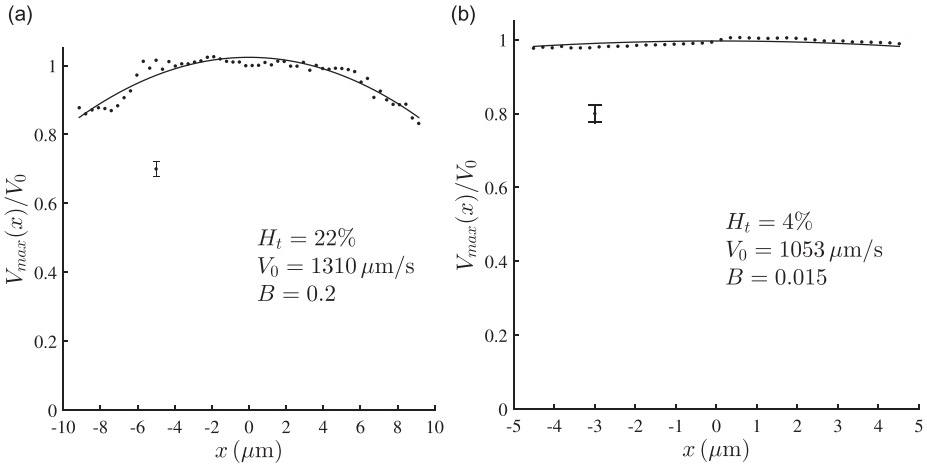

FIG. 4. RBC maximal velocity profiles in a $20\,\mu\text{m} \times 20\,\mu\text{m}$ (a) and $10\,\mu\text{m} \times 10\,\mu\text{m}$ (b) microchannel. Dots: velocity data normalized by V_0; Solid line: best fitting adjustment to Equation (2). For sake of clarity, the uncertainty on each velocity measurement by dual-slit is indicated on a single isolated point (not a real data point). The uncertainty on the V_0 value obtained is $\pm 0.05 \times V_0$.[40] The best-fitting values of V_0 and B are indicated on the graph, as well as the tube hematocrit H_t.

with H_t nor V_0 could be extracted from this data set, with a large dispersion found in B values corresponding to similar flow conditions.

Despite dispersion, these results show that the RBC velocity profiles in square microchannels for various flow parameters are described correctly by Equation (2), first suggested for a cylindrical channel *in vivo*.[29] Thus, this equation appears suitable as a reference profile for RBCs, instead of the no-slip velocity profile of a Newtonian fluid generally used in the previous studies.[1,19,30] Moreover, the bluntness of this velocity profile is highly dependent on the channel size, with flat RBC profiles ($B = 0.02 \pm 0.03$) obtained when the RBCs are confined ($10\,\mu\text{m} \times 10\,\mu\text{m}$ channels) and more blunted ones when RBCs are less confined ($B = 0.25 \pm 0.12$) in $20\,\mu\text{m} \times 20\,\mu\text{m}$ channels. The increasing value of B with increasing channel size is consistent with the PIV measurements in larger ($100\ \mu\text{m}$) microchannels where a slip velocity of order $0.5V_0$ was observed, corresponding to B around 0.5 (Ref. 47), and with the two-photon measurements performed *in vivo* in a 50-μm diameter microvessel in the brain, where a similar value has been obtained for B (see Fig. 1 in Ref. 43).

B. Validation of RBC and suspending fluid flow rates measurements

1. RBC flow rate

As explained in Section II B 3, the RBC flow rate can be obtained from the RBC velocity profile and hematocrit measurements through the use of Equation (4). When the RBC suspension is sufficiently diluted, this indirect measurement of the RBC flow rate can be compared with the reference method, based on RBC counting, see Equation (5). The results presented in Figure 5 shows a reasonable agreement between both measurement methods. The average of the absolute value of the relative difference between the measured RBC flow rate values and the reference ones is 19%. This validates the present measurement technique of the RBC flow rate and justifies *a posteriori* the assumptions implied in the derivation of Equation (4), about the way the RBC velocity and hematocrit profile are determined.

2. Validation of flow rate measurements by verification of mass conservation

We now turn to the validation of the flow rate measurement techniques presented in the present paper by verifying that the results obtained are consistent with mass conservation of both suspending fluid and RBCs at micro-bifurcations.

To that end, we compare the sum of the flow rates measured in each daughter branches of a bifurcation with the flow rate measured in the feeding branch. Results are shown in Figure 6(a) for the RBC flow rate, and, similarly, in Figure 6(b) for the suspending fluid flow rate. The

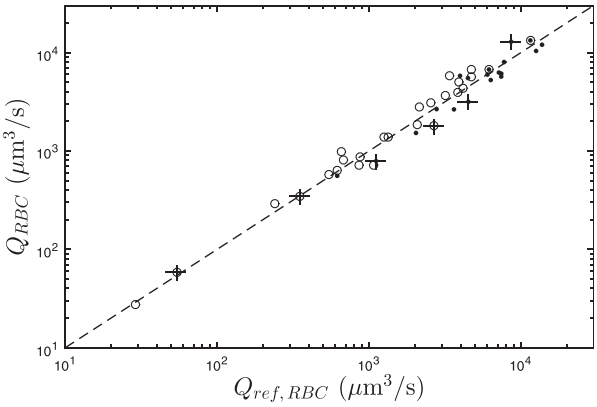

FIG. 5. RBC flow rate obtained from Equation (4) as a function of a reference RBC flow rate value obtained by counting. Circles: measurements in $10\,\mu\text{m} \times 10\,\mu\text{m}$ microchannels; Dots: measurements in $20\,\mu\text{m} \times 20\,\mu\text{m}$ microchannels; Dashed line: identity function. The error bars are shown for a limited set of data points only, for sake of clarity. The error bars on $Q_{ref,RBC}$ come from the RBC-counting error and are $\pm 0.15 \times Q_{ref,RBC}$. The error bars on Q_{RBC} are mainly caused by experimental errors on the determination of V_0 and H_t, see Equation (4) and are $\pm 0.17 \times Q_{RBC}$.

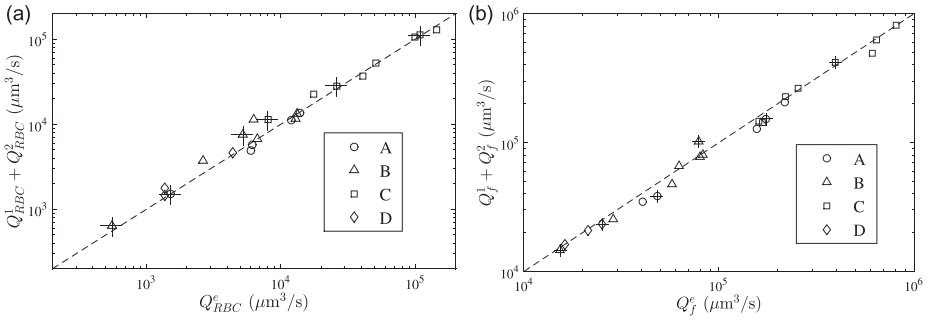

FIG. 6. (a) Sum of the RBC flow rates measured in the daughter branches of a bifurcation, $Q^1_{RBC}+Q^2_{RBC}$, compared with the RBC flow rate measured in the feeding branch, Q^e_{RBC}. (b) Sum of the suspending flow rates measured in the daughter branches of a bifurcation, $Q^1_f+Q^2_f$, compared with the suspending fluid flow rate measured in the feeding branch, Q^e_f. The different labels correspond to different types of micro-bifurcations.

agreement between incoming and outgoing flow rates is good, both for RBC and suspending fluid flow rates. In particular, the results presented in Figure 6(b) demonstrate that the method developed here to obtain the suspending fluid flow rate from the measurement of the RBC velocity profile is consistent with mass conservation.

An apparent deviation from mass conservation parameter can be calculated for each data point as

$$E_i = \frac{|Q^e_i - (Q^1_i + Q^2_i)|}{Q^e_i}, \tag{7}$$

where Q^e_i is the flow rate in the inlet branch, Q^1_i and Q^2_i are the flow rates in the outlet branches, and i is either "*RBC*" for RBC flow rates or "*f*" for suspending fluid flow rates. This parameter represents half the absolute uncertainty on corresponding fractional flows in both branches of the bifurcation (i.e., $\Delta\left(\frac{Q^1_i}{Q^e_i}\right)$ and $\Delta\left(\frac{Q^2_i}{Q^e_i}\right)$), assuming that this uncertainty is equal in both branches. In fact, in this case, because of mass conservation

$$\frac{Q^1_i + Q^2_i}{Q^e_i} = 1 \pm 2\Delta\left(\frac{Q^1_i}{Q^e_i}\right) = 1 \pm 2\Delta\left(\frac{Q^2_i}{Q^e_i}\right), \tag{8}$$

leading to

$$\Delta\left(\frac{Q^1_i}{Q^e_i}\right) = \Delta\left(\frac{Q^2_i}{Q^e_i}\right) = \frac{1}{2}\left|1 - \frac{Q^1_i + Q^2_i}{Q^e_i}\right| = \frac{1}{2}E_i. \tag{9}$$

The mean values for E_i are given in Table II for the four types of bifurcations studied. For microbifurcations A, B, and D, they are in the range 5%–15%, showing that the methods developed to measure blood flows in microchannels, based on the measurement of hematocrit and velocity profiles, are accurate. The slightly larger measurement errors for the bifurcations of type *C* are explained *a posteriori* because the dual-slit measurement was optimized (in terms of number of images and frame acquisition rate) for the flow in the outlet channels and not for the feeding branch where the flow rate is two times smaller and thus the optimal dual-slit conditions are more difficult to achieve. This led to an underestimation of the velocity and thus the flow rate in the feeding branch.

3. Discussion on the assumptions made about the suspending fluid velocity profile

Because it is still not feasible to simultaneously measure the velocity profiles of both red blood cells and suspending fluid in channels of capillary size or slightly larger, assumptions

TABLE II. Mean values of the experimental relative errors E_{RBC} and E_f between incoming and outgoing flow rates at a bifurcation as a function of the micro-bifurcation type. The number of experiments taken into account is given in the last line of the table.

$\langle E_i \rangle$ (%)	A	B	C	D
$\langle E_{RBC} \rangle$	14.0	13.7	27.2	6.7
$\langle E_f \rangle$	3.6	7.4	10.5	14.5
# Exp.	3	8	7	5

have been made in Section II B 3 regarding the suspending fluid velocity profile. This velocity profile must of course satisfy to the no-slip condition at channel walls and, consistently with experimental results obtained in larger channels with low RBC concentrations,[16] is very unlikely to display velocities larger than the maximal velocity of RBCs. In the present work, because the suspending fluid is Newtonian, we assumed the velocity profile of a Newtonian fluid (i.e., a profile that would be parabolic in a cylindrical channel) with zero velocity at walls and maximal velocity equals to V_0, the maximal velocity of RBCs. Alternatively, inspired from the classical two-layer modeling for blood flow in narrow channels (e.g., Ref. 44), where the outer layer represents the CFL and only consists of plasma and the inner region with higher viscosity represents flowing RBCs mixed with plasma, we could have assumed that the suspending fluid displays a highly sheared Newtonian profile in the outer region and then matches with the measured RBC velocity profile. But this would imply adding another unknown parameter, i.e., the thickness of the CFL, which is also not possible to measure in our experimental conditions due to light diffraction (see Section II B). Another possible assumption, while less realistic because it does not respect the no-slip condition at walls, has been made by Sherwood *et al.*[46] who matched the suspending fluid with the measured RBC velocity profile throughout the channel depth.

Any realistic velocity profile would lie in between the latter and the one considered in the present study. It is not possible to directly discriminate between these assumptions on experimental bases, as both of them lead to conservation of the suspending fluid within experimental error at diverging bifurcations. In the present study, mass conservation of the suspending fluid has indeed been demonstrated in Figure 6(b), which supports the assumption made. Mass conservation of the suspending fluid, however, would also directly derive from RBC conservation, demonstrated in Figure 6(a), if the suspending fluid velocity was assumed to be equal to the measured RBC velocity profile. An indirect evidence in favor of the assumption made in the present study can be obtained by studying the dependence of the discharge hematocrit $H_d = Q_{RBC}/Q_{blood}$ as a function of the tube hematocrit H_t. This dependence is plotted in Figure 7, allowing to characterize the so-called Fåhræus effect. Our experimental data for both $10\,\mu$m $\times 10\,\mu$m and $20\,\mu$m $\times\, 20\,\mu$m are in quantitative agreement with empirical correlations obtained by Pries *et al.*[36] for capillary tubes with circular cross-sections, using the hydraulic diameter D_h instead of the tube diameter (for the square cross-section channels considered here, $D_h = W$) and dividing the coefficients by a factor of 0.86 in order to account for the difference in characteristic size between human and rat RBCs, as proposed by Lorthois *et al.*[21] This strongly supports the assumptions made about the suspending fluid velocity profile in the present study. By contrast, matching the suspending fluid and RBC velocity profiles is not consistent with the observed RBC slip velocity at walls and would result in $H_t = H_d$, i.e., no Fåhræus effect.

4. Flow rate measurement accuracy: Comparison with in vivo data

In vivo data have been compiled by Cokelet *et al.*[6] in order to quantify the experimental errors by reporting the observed deviations from the principle of mass conservation. These authors analyzed the ratio between incoming and outgoing RBC flow rate at a bifurcation compared with the ratio of incoming and outgoing whole blood flow rate, i.e., $Q^e_{RBC}/(Q^1_{RBC} + Q^2_{RBC})$ vs $Q^e_{blood}/(Q^1_{blood} + Q^2_{blood})$. They have shown that these ratios vary from 0.1 to 10, which

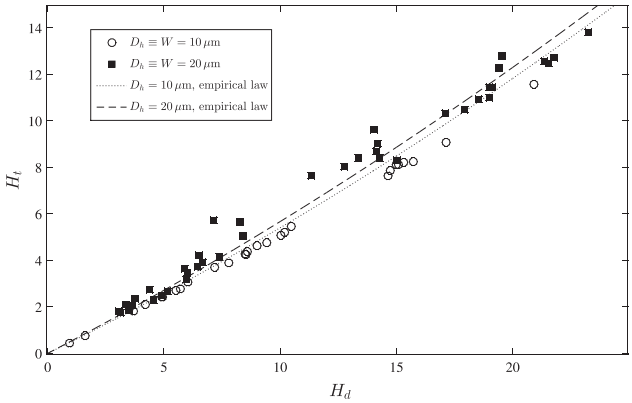

FIG. 7. Relation between the tube hematocrit H_t and the discharge hematocrit $H_d = Q_{RBC}/Q_{blood}$. Circles: data points obtained in $10\,\mu\text{m} \times 10\,\mu\text{m}$ microchannels; Black squares: data points for $20\,\mu\text{m} \times 20\,\mu\text{m}$ microchannels. Lines: empirical law adapted from Pries *et al.*,[36] $H_t/H_d = H_d + (1 - H_d)(1 + 1.7\exp(-0.483D_h) - 0.6\exp(-0.013D_h))$, with $D_h = 10\,\mu$m (dotted line) and $D_h = 20\,\mu$m (dashed line).

corresponds to very large measurement errors. We compared these *in vivo* data with the *in vitro* data obtained in the present study, see Figure 8. Our experimental points lie close to unity. This result shows that the methodologies developed to measure blood and RBC flows in the present work are reliable and much more accurate than previous *in vivo* data. This is not surprising as such a better accuracy, compared with *in vivo* studies, is the main motivation behind the use of a microfluidic-based approach for the study of the phase separation effect. Its potential for studying steady state phase separation effect is demonstrated in Section III C below.

C. Phase separation effect: Present results and comparison with previous empirical and *ad hoc* parametric descriptions

In the present section, the framework used for analyzing the phase separation effect is first introduced, highlighting the similarities and differences with the methodological framework of Pries *et al.*[33,37] The main features of the phase separation behavior as predicted by the most recent version of their empirical law[33] and by the *ad hoc* law proposed by Gould and Linninger[12] are also summarized. Then, a parametric study of the effect of hematocrit on phase separation is presented for a limited set of bifurcation geometries, including symmetrical and

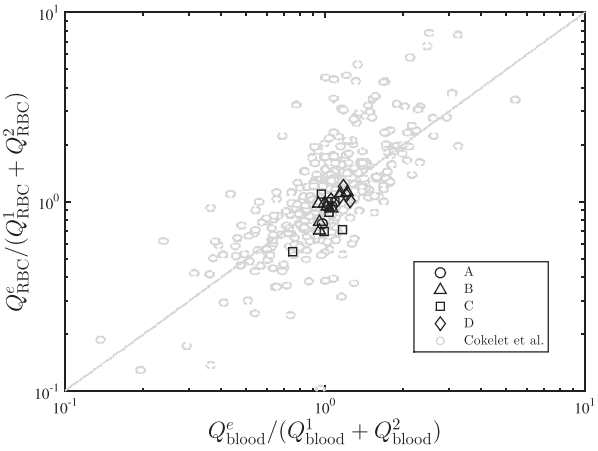

FIG. 8. Deviation from mass conservation: ratio between incoming and outgoing RBC flow rate at a bifurcation, $Q^e_{RBC}/(Q^1_{RBC} + Q^2_{RBC})$, compared with the ratio of incoming and outgoing whole blood flow rate, $Q^e_{blood}/(Q^1_{blood} + Q^2_{blood})$. Black symbols: *in vitro* data for our four types of microbifurcations, grey symbols: *in vivo* data compiled by Cokelet *et al.*[6]

asymmetrical ones. Despite the dispersion of the obtained results, some interesting behaviors emerge, which are subsequently discussed by comparison with these two previous parametric descriptions.

1. Methodological framework and reference phase separation laws

Following Pries *et al.*,[37] the heterogeneity of hematocrit in a given microbifurcation is characterized in two different ways. The first one focuses on the deviation from unity of the relative discharge hematocrits ($\frac{H_d^i}{H_d^e}$) in both outlet branches i. However, mass conservation does not lead to a trivial relationship between these two parameters. Because phase separation vanishes when the proportion of RBCs flowing from the inlet branch to a given outlet branch is equal to the proportion of the blood flowing from the inlet branch to this same outlet branch, the second one focuses on the deviation of the fractional RBC flows in each daughter branch of the bifurcation, FQ_{RBC}^i, from the fractional blood flow entering the same branch, FQ_{blood}^i. Mass conservation obviously leads to $FQ_{RBC}^1 + FQ_{RBC}^2 = 1$ and $FQ_{blood}^1 + FQ_{blood}^2 = 1$, and any parametrization of the phase separation effect based on these parameters must exhibit a central symmetry around point (0.5, 0.5).

Thus, based on the previous experimental findings, Pries *et al.*[33] introduced a *logit* function that reproduces the observed sigmoid shape of the experimental measurements and a threshold value X_0 for the fractional blood flow entering a given daughter branch below which no RBC enters this same branch

$$FQ_{RBC}^i = \begin{cases} 0 & \text{if } FQ_{blood}^i < X_0 \\ 1 & \text{if } FQ_{blood}^i > 1 - X_0 \\ \dfrac{1}{1 + e^{-\left(A + B\ logit\left(\frac{FQ_{blood}^i - X_0}{1 - 2X_0}\right)\right)}} & \text{else,} \end{cases} \tag{10}$$

where $logit(x) = ln\left(\frac{x}{1-x}\right)$ and A, B, and X_0 are non-dimensional parameters given by $X_0 = \underline{X}_0 \times (1 - H_d)/D_h^e$ with $\underline{X}_0 = 1.12\,\mu$m; $A = -\underline{A} \times \frac{D_h^1 - D_h^2}{D_h^1 + D_h^2} \times (1 - H_d)/D_h^e$ with $\underline{A} = 15.47\,\mu$m; and $B = 1 + \underline{B} \times (1 - H_d)/D_h^e$ with $\underline{B} = 8.13\,\mu$m. Note that, as previously, the numerical values of the coefficients used in these expressions have been divided by a factor of 0.86 in order to account for the difference in characteristic size between human and rat RBCs. As these parameters vary linearly with the discharge hematocrit, a smooth evolution of the phase separation effect with H_d is expected from this parametrization, from maximal separation in the limit of small hematocrits to no phase separation in the limit of very large hematocrits.

On the contrary, Gould and Linninger[12] proposed a simpler formulation, written as

$$FQ_{RBC}^i = \frac{1}{1 + \left(\dfrac{1}{FQ_{blood}^i} - 1\right)\left(\dfrac{A_i}{A_j}\right)^{1/M}}, \tag{11}$$

where A_i and A_j are the cross-sectional areas of both daughter branches and M is a single adjustable "drift" parameter introduced to account for the extent of plasma skimming at the bifurcation. Because experimental data were lacking to propose an improved parameterization for the value of this parameter as a function of bifurcation geometry, the value of 5.25 has been proposed, corresponding to the best adjustment to the *in vivo* experimental data previously obtained by Pries *et al.*[37] in a bifurcation for which the feeding vessel diameter is 7.5 μm and the daughter branches diameters are 6 and 8 μm, respectively.

While according to Gould and Linninger,[12] this parametrization matches the empirical fractional blood flows acquired in this single bifurcation "no worse" than the previous one, they behave both qualitatively and quantitatively in very different ways. In particular, in the latter,

the phase separation behavior in each branch has no inflection point, implying that the largest daughter branch always receives a larger proportion of the inflowing RBCs whatever the blood flow in this daughter branch. Moreover, it predicts a proportional distribution of RBCs and blood in both branches of the bifurcation when their cross-sectional areas are equal. Thus, according to this law, the phase separation effect should vanish in symmetrical bifurcations. Finally, it does not depend on the discharge hematocrit.

Before turning to the comparison of these descriptions with our experimental results, it is worth noting that, as pointed out by Pries *et al.*,[37] the original experimental data, because they are acquired for all three vessel segments of a given bifurcation, contain redundant information that can be used to correct these data so that the equations of mass conservation are satisfied (see Equations (2)–(12) in Ref. 37). By contrast, in the present study, the raw experimental values will be kept in order to avoid the introduction of any non-controlled bias in the analysis, except when stated explicitly otherwise. For each acquisition, the absolute errors on the fractional (blood or RBC) flow rates in each branch will be estimated to be half of E_{blood} or E_{RBC}, the parameters characterizing deviations from mass conservation, see Equation (7). As indicated previously, this comes down to assume that the average error is equal for all branches.

2. Influence of hematocrit and bifurcation geometry

In order to study the effect of hematocrit and bifurcation geometry on phase separation, the parameters that were varied are the microchannel sizes (4 kinds of micro-bifurcations, see Table I), the tube hematocrit (2%–20%), the input flow rate, which depends on the pressure gradients imposed, from $Q^e_{blood} = 7 \times 10^3\ \mu m^3/s$ to $Q^e_{blood} = 8.5 \times 10^5\ \mu m^3/s$, and the asymmetry of the output flows, which also depends on the pressure gradients imposed, from $Q^1_{blood}/Q^2_{blood} = 0$ to $Q^1_{blood}/Q^2_{blood} = 1$.

The fractional RBC flow in each branch of the bifurcation was deduced and plotted as a function of the fractional blood flow in the same branch, evidencing their deviation from identity. Figure 9, main panels, displays the results obtained in symmetrical bifurcations (bifurcations A, B, and C) for inlet tube hematocrits below 5% (left column) and over 5% (right column). Insets display the variations of discharge hematocrit in each branch of the bifurcation relative to inlet as a function of the fractional blood flow in the same branch, evidencing their deviation from unity.

For all these symmetrical bifurcations, when the inlet tube hematocrits are below 5%, which correspond to a discharge hematocrits approximately below 9% (see Figure 7), both the shape and order of magnitude of the phase separation effect are consistent with the empirical description proposed by Pries *et al.*[33] Regarding the shape, most of the experimental points are located below the identity line when the fractional blood flow is below 0.5 (except one in bifurcations A and B and two in bifurcation C) and above the identity line when the fractional blood flow is above 0.5 (with the same number of exceptions). In other words, the daughter branch with smallest flow receives a lower fraction of inflowing RBCs than the daughter vessel with largest flow, which is consistent with an inflection point in the description of phase separation. Regarding the magnitude, the phase separation behavior as predicted by Equation (10) in the limit of low hematocrits (continuous lines) lays in between the experimental points. It is even almost superimposed with the experimental points, except a pair of outliers in bifurcation C, when they are corrected following Ref. 37 so that the equations of mass conservation are satisfied, see Figure 10. Altogether, even with an improved parameterization for the value of the drift parameter as a function of bifurcation geometry, the *ad hoc* description introduced by Gould and Linninger[12] would be ineffective to describe phase separation in these symmetrical bifurcations at low hematocrit.

When the hematocrit increases above 5%, the experimental points lay much closer to the identity line, suggesting a stronger decrease of the phase separation effect with increasing RBC concentration than predicted by Pries *et al.*[33] This can be quantified by the decrease of the rms deviation of the experimental points to the identity line, from 0.12 to 0.07 for bifurcation A, from 0.16 to 0.06 for bifurcation B, and from 0.26 to 0.05 for bifurcation C. In this last

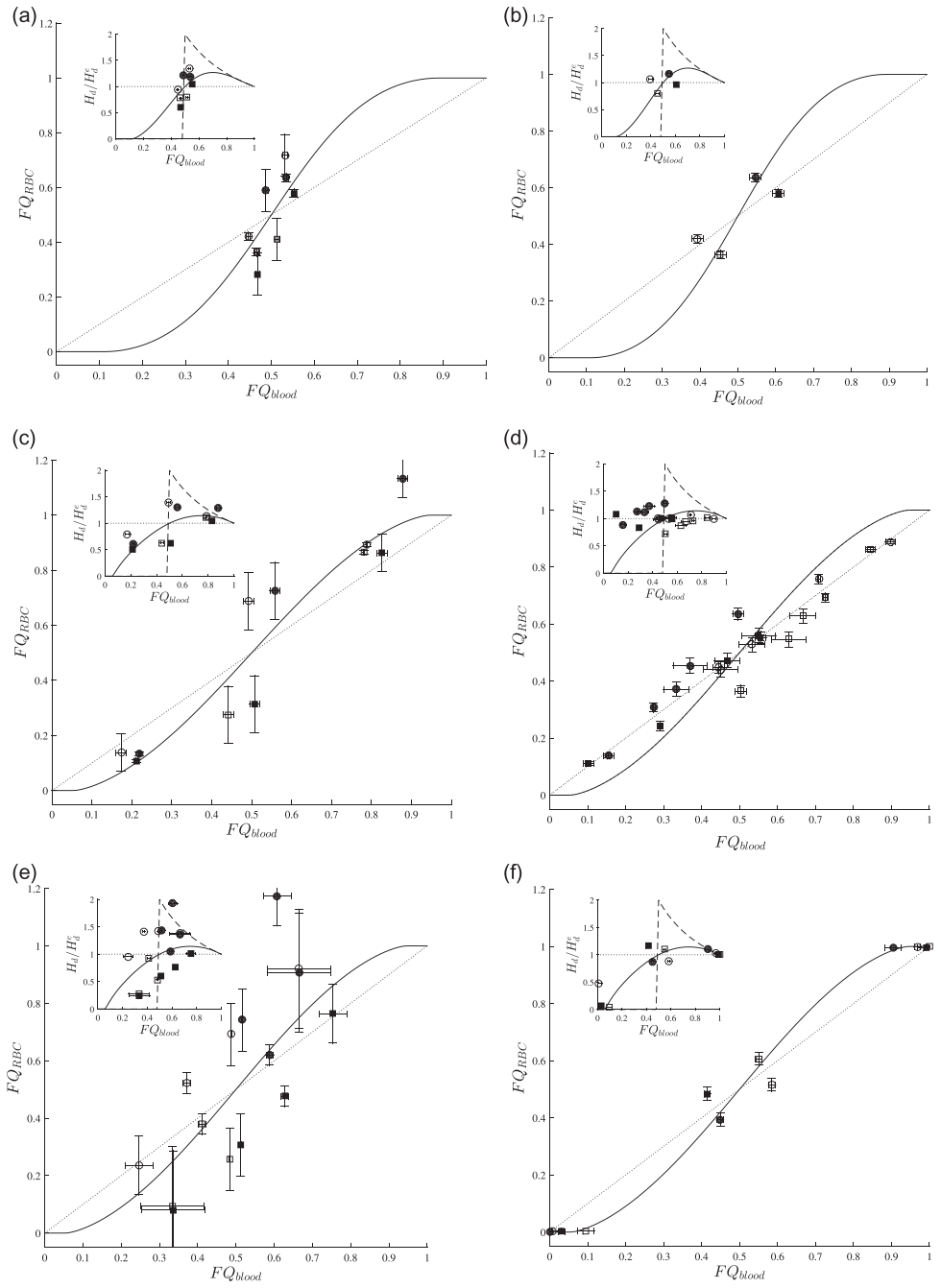

FIG. 9. Phase separation in symmetrical bifurcations: influence of inlet tube hematocrit (left: below 5%; right: above 5%). Upper row: bifurcation A; Middle row: bifurcation B, Lower row: Bifurcation C. Main panels: fractional RBC flow as a function of fractional blood flow in the same branch. Insets: ratio of discharge hematocrit in daughter branch relative to inlet branch as function of fractional blood flow in the same daughter branch. Filled symbols: outlet channel 1; Open symbols: outlet channel 2; Circles: original data; Squares: images of original data by central symmetry around (0.5, 0.5). The error bars correspond to $E/2$, as given by Equation (7). Continuous line: Pries *et al*. empirical law[33] in the limit of small hematocrits. Dotted line: Proportional repartition of blood and RBCs (no phase separation). Dashed line in insets: maximal phase separation (all RBCs flowing in the channel with highest flow).

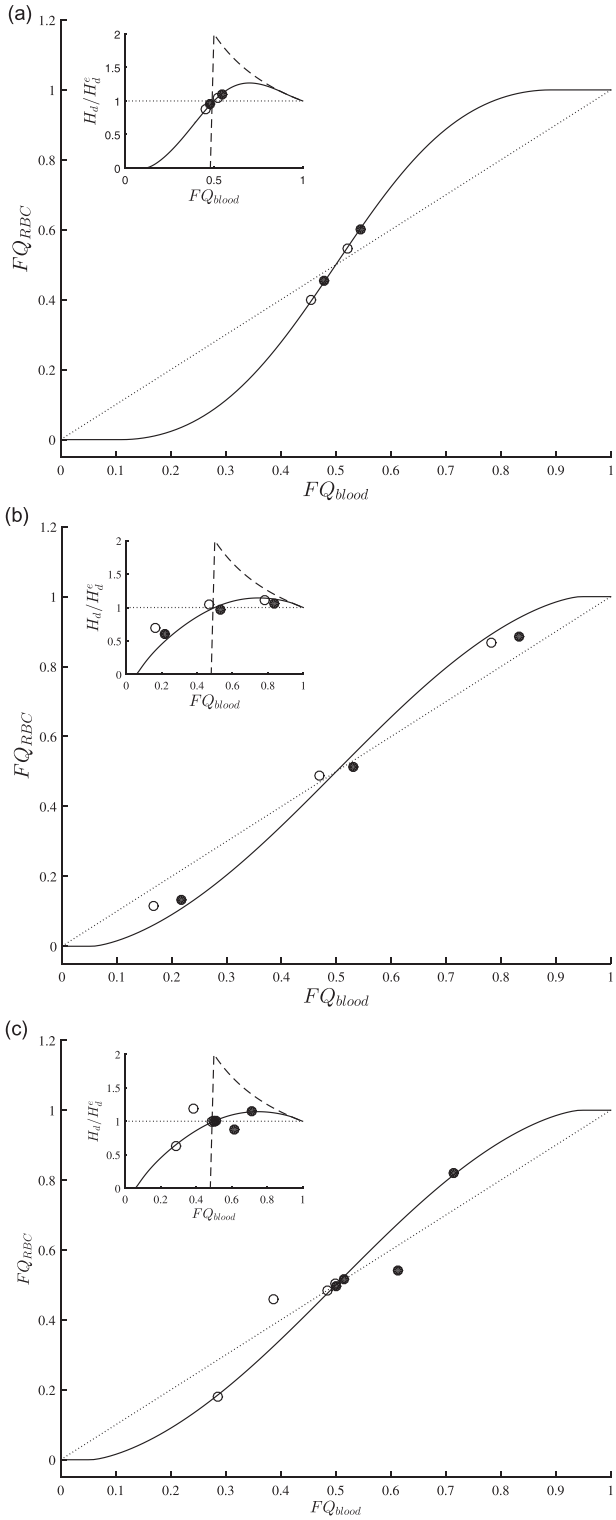

FIG. 10. Phase separation in symmetrical bifurcations for inlet tube hematocrits below 5%. Upper row: bifurcation A; Middle row: bifurcation B, and Lower row: Bifurcation C. Same conventions as in Figure 9 except that experimental data have been corrected following Eqs. (2)–(12) in Ref. 37 so that blood and RBC mass conservation are satisfied at each bifurcation and that the images of corrected data by central symmetry around (0.5, 0.5) are not shown because they are exactly superimposed to the corrected data.

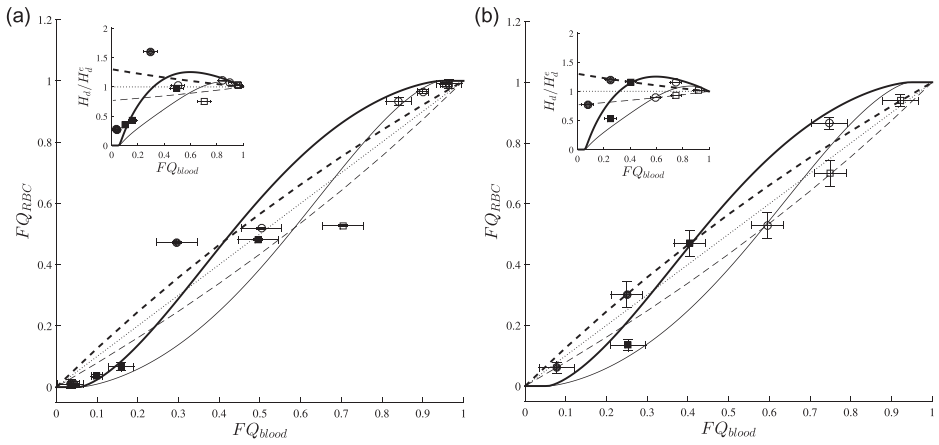

FIG. 11. Phase separation in the asymmetrical bifurcation D: influence of hematocrit. Same conventions as in Figure 9, except that bold lines correspond to predictions of phase separation laws for outlet branch 1 and thin lines for outlet branch 2, and that dashed lines represent Gould and Linninger[12] *ad hoc* phase separation law.

bifurcation, and despite the decrease in phase separation, the existence of a flow threshold below which no RBCs enter the corresponding daughter branch is confirmed (see Figure 9(f), where experimental points with fractional blood flow below 10% or above 90% correspond to 0% or 100% fractional RBC flow, respectively).

Figure 11 displays the results obtained for the asymmetrical bifurcation D. As previously, when the inlet tube hematocrits are below 5%, both the shape and order of magnitude of the phase separation effect are consistent with the empirical description proposed by Pries *et al.*[33] (continuous lines). However, in this case, increasing the hematocrit does not reduce the rms deviation of the experimental points to the identity line, which remains unchanged (with the rms deviation from identity line varying from 0.07 at low hematocrit to 0.09 at larger ones). Thus, no drastic reduction in phase separation is observed.

In addition, the phase separation amplitude is also close to the *ad hoc* prediction of Gould and Linninger (dashed lines). The rms deviation from their *ad hoc* law is 0.09 whatever the hematocrit, i.e., even slightly smaller than the 0.12 rms deviation from Pries' law, although the strong decrease of discharge hematocrit with fractional blood flow in the largest daughter branch observed experimentally (see Figure 11(a)) is not well captured by the *ad hoc* description. This is more clearly seen in inset (bold dashed line) where the *ad hoc* description leads to a relative increase of the discharge hematocrit in the largest branch whatever its fractional blood flow, while the experimental points corresponding to low fractional blood flows clearly have values below unity.

IV. CONCLUSIONS AND FUTURE WORK

The experimental approach introduced in the present paper enables the study of steady state RBC phase separation in microfluidic bifurcations with sizes below 20 μm, for a large range of inlet discharge hematocrits. As discussed in Section I, this is very challenging and had never been achieved before. We argued that a careful cross-validation of different measurement techniques, which indeed relies on strong simplifying assumptions, is required to achieve a quantitative evaluation of the phase separation effect in such small channels. Using this point of view, these assumptions have been validated. In particular, we have shown that the RBC flow rate can be estimated from four independent parameters: the channel width W, the tube hematocrit H_t, the maximal RBC velocity V_0, and the bluntness B of the maximal RBC velocity profile. The optimized dual-slit technique, because it allows the direct measurement of V_0 and B without any calibration, is thus particularly adapted in this context. Moreover, we have shown that the suspending fluid flow rate can be accurately evaluated without the use of any additional

extrinsic tracers by assuming the velocity profile of a Newtonian fluid with no-slip at walls and maximal velocity equal to the maximal velocity of RBCs. Contrarily to other possible assumptions encountered in the literature, the present assumption is consistent with the mass conservation of the suspending fluid at bifurcations but does not automatically derive from RBC mass conservation. (As discussed previously, mass conservation of the suspending fluid would also derive from RBC mass conservation if the suspending fluid velocity was assumed to be equal to the measured RBC velocity profile.) The present assumption is also consistent with the previous knowledge on the Fåhræus effect.

It is noteworthy that these methodological advances take place while, in parallel, efficient simulation methods are emerging to study phase separation of multi-RBC systems in small channels in three dimensions,[14,18,25] which is also highly challenging.[11] We believe that, in the future, cross-fertilization between these experimental and computational approaches will lead to fantastic breakthroughs, the experiments providing insight on the phenomenology and reference data needed to validate the simulations and calibrate their input parameters, and the simulations enabling the study of situations that cannot be experimentally reproduced or of parameters that cannot be experimentally measured, e.g., the trajectory of individual RBCs or the mean velocity profile of the suspending fluid. In particular, in order to gain a deeper understanding of the mechanisms at play, including how the control parameters affect the relative contributions of *plasma skimming*, i.e., the inhomogeneous RBC distribution across the upstream channel, and *red cell screening*, i.e., the trajectories of RBCs vs. suspending fluid in the vicinity of the bifurcation,[35] going back and forth between experimental and simulation approaches will be necessary.

In both cases, strong simplifications are present by comparison to *in vivo* situations. In experiments, these simplifications concern shapes (straight square channels branching at right angles vs. curvilinear cylindrical vessels lined with endothelial cells and branching at larger angles[3,24]), physico-chemical properties of the surface in contact with blood (non specific adsorption of bovine serum albumin vs. presence of the endothelial surface layer with glycocalyx[17]), cell types (absence vs. presence of platelets and white blood cells), and suspending fluid (absence vs. presence of plasma proteins mediating RBC aggregation[46,47]), while in simulations, the shapes are more realistic, with cylindrical channels possibly branching with realistic angles.[25] Note that the methodological developments presented here could be used to study the impact of some of these simplifications, e.g., by using autologous plasma for RBC resuspension, adding a controlled amount of platelets or white blood cells, or taking advantage of new micro-fabrication techniques (e.g., Ref. 7) to built more realistic geometries and/or functionalize the channels with polymer brushes mimicking the effect of the endothelial surface layer, in the same spirit as Lanotte *et al*.[17]

The main results of this study, besides methodological validation, are the following. First, two different families of RBC velocity profiles in $10\,\mu\text{m} \times 10\,\mu\text{m}$ and $20\,\mu\text{m} \times 20\,\mu\text{m}$ channels have been observed, the first ones being very flat ($B = 0.02 \pm 0.03$) whatever the hematocrit and maximal RBC velocity and the second ones being significantly more blunted ($B = 0.25 \pm 0.12$) but always exhibiting a large RBC slip at walls. This provides a new information about the dynamics of the system, which had been previously overlooked because of the difficulties of near wall velocity measurements, but might be very useful for numerical validation. We believe that the transition between these two regimes is linked to the RBC spatial organization in the channel, from single- to multi-file flows to highly packed RBCs, which is expected to be highly dependent on the confinement and to occur for channel to RBC size ratios around one. Further investigation is needed to determine the transition threshold. Such a transition might play a role to understand the differences in phase separation behavior in the present asymmetrical bifurcation, where RBCs flow in these two regimes simultaneously take place in either daughter branches, which is not the case in the symmetrical bifurcations.

Second, the results obtained on phase separation provide new, even yet incomplete, reference data obtained in controlled conditions in a regime where *in vitro* results are still lacking. These data clearly show that the *ad hoc* law proposed by Gould and Linninger[12] is

inappropriate for parametrizing the phase separation effect. By contrast, they are consistent with the empirical description of Pries *et al.*[33,37] at low hematocrits. This might be surprising with regard to the strong simplifications of the present *in vitro* approach by comparison to *in vivo* situations mentioned above. Thus, these differences do not play a fundamental role in the physics of phase separation, at first order, as far as averaged quantities are concerned, when interactions of RBCs with other RBCs and the vessel wall are weak. This might no longer be the case when these interactions become stronger. Our results indeed suggest an unexpected decrease of phase separation with increasing hematocrit in symmetric bifurcations by comparison with the *in vivo* results.[37] However, a strong reduction of phase separation with increasing hematocrit has also been recently reported in several three-dimensional simulation studies based on different approaches. A diminution in separation efficiency with increasing hematocrit has been reported in Refs. 18 and 25 where a dissipative particle dynamics and new open boundary conditions have been introduced and validated by comparison with convincing benchmark simulations. A stronger reduction has been reported in Ref. 14 where a Lattice-Boltzmann/Immersed-boundary method was used to study symmetrical bifurcations with branches with circular cross-sections and 10 μm diameters. Unfortunately, a quantitative comparison with these results is not possible. In fact, in the latter method, the difficulty in imposing appropriate boundary conditions was not addressed. Thus, the authors artificially increased the Reynolds number in order to "accommodate a decrease in the computational load" by reducing the inlet length needed to obtain an equilibrium parachute-like shape of the injected RBCs, and only considered the transient passage of 10 successive cells in a fluid-filled bifurcation. Moreover, in the former approach, the fractional blood flow change was achieved by changing the diameters of the daughter branch, even if the most recent version of this approach enables the bifurcation geometry and fractional blood flow to be fixed independently. In the future, this approach might be very powerful to help understand whether differences in the details of the channel geometry (e.g., square versus cylindrical channels) can explain the unexpected reduction of phase separation with increased hematocrit observed in the present study.

Despite the methodological advances presented here, the experimental variability is still surprisingly high. This variability might be linked to several experimental difficulties encountered when dealing with highly confined RBC flows in a large range of concentrations. First, the shape of the hematocrit profile, which has not been possible to measure up to now, is important for characterizing the CFL thickness and its influence on the phase separation effect. It might depend on the confinement regime (see above). Second, in the channel size range under study, it was extremely difficult to control the inlet tube and/or discharge hematocrit as a function of the feed hematocrit. Transient effects might play a role here, once again influencing the shape of the hematocrit profile and the thickness of the CFL. This might explain the large dispersion in RBC velocity profile bluntness we measured in the present study and might in turn influence the phase separation effect. Thus, improving the design of the injection channel and developing a technique allowing the hematocrit profile to be measured in small channels are needed to perform a comprehensive parametrical study of the phase separation effect. This was beyond the scope of this paper but will be the object of future work. However, variability might also be intrinsically linked to the phase separation phenomenology, requiring a probabilistic description to be introduced for further improving the accuracy of numerical simulation of the coupling between network architecture and blood flow dynamics at large scale in microcirculation.

ACKNOWLEDGMENTS

We gratefully acknowledge D. Bourrier, M. Dilhan, and P. Joseph from LAAS-CNRS, Toulouse for their help in the microfabrication and microfluidic experiments, and Sébastien Cazin from IMFT for his help in image acquisition and post-processing. Sophie Roman was the recipient of a doctoral fellowship from the Institut National Polytechnique de Toulouse. This work has been partially supported by ERC Consolidator BrainMicroFlow (GA 615102), GDR CNRS 2760 Biomécanique des fluides et des transferts: Interactions Fluide Structure Biologique, BQR INPT

2011 (VLAN Project), the French RENATECH network, and by the Fermat Research Federation (FR INPT-UT3-CNRS-INSA Toulouse 3089).

[1]M. Baker and H. Wayland, "On-line volume flow rate and velocity profile measurement for blood in microvessels," Microvasc. Res. **7**, 131–143 (1974).
[2]R. T. Carr and L. L. Wickham, "Influence of vessel diameter on red-cell distribution at microvascular bifurcations," Microvasc. Res. **41**, 184–196 (1991).
[3]F. Cassot, F. Lauwers, S. Lorthois, P. Puwanarajah, V. Cances-Lauwers, and H. Duvernoy, "Branching patterns for arterioles and venules of the human cerebral cortex," Brain Res. **1313**, 62–78 (2010).
[4]B. Chayer, K. L. Pitts, G. Cloutier, and M. Fenech, "Velocity measurement accuracy in optical microhemodynamics: Experiment and simulation," Physiol. Meas. **33**, 1585–1602 (2012).
[5]B. Chen, F. Guo, and H. Xiang, "Visualization study of motion and deformation of red blood cells in a microchannel with straight, divergent and convergent sections," J. Biol. Phys. **37**, 429–440 (2011).
[6]G. Cokelet, A. Pries, and M. Kiani, "Observations on the accuracy of photometric techniques used to measure some *in vivo* microvascular blood flow parameters," Microcirculation **5**, 61–70 (1998).
[7]R. Courson, S. Cargou, V. Conedera, M. Fouet, M. C. Blatche, C. L. Serpentini, and A. M. Gue, "Low-cost multilevel microchannel lab on chip: DF-1000 series dry film photoresist as a promising enabler," RSC Adv. **4**, 54847–54853 (2014).
[8]J. W. Dellimore, M. J. Dunlop, and P. B. Canham, "Ratio of cells and plasma in blood flowing past branches in small plastic channels," Am. J. Physiol. **244**, 635–643 (1983).
[9]M. Desjardins, R. Berti, J. Lefebvre, S. Dubeau, and F. Lesage, "Aging-related differences in cerebral capillary blood flow in anesthetized rats," Neurobiol. Aging **35**, 1947–1955 (2014).
[10]B. M. Fenton, R. T. Carr, and G. R. Cokelet, "Nonuniform red-cell distribution in 20 to 100 μm bifurcations," Microvasc. Res. **29**, 103–126 (1985).
[11]J. B. Freund, "Numerical simulation of flowing blood cells," Annu. Rev. Fluid Mech. **46**, 67–95 (2014).
[12]I. G. Gould and A. A. Linninger, "Hematocrit distribution and tissue oxygenation in large microcirculatory networks," Microcirculation **22**, 1–18 (2015).
[13]R. Guibert, C. Fonta, and F. Plouraboue, "A new approach to model confined suspensions flows in complex networks: Application to blood flow," Transp. Porous Media **83**, 171–194 (2010).
[14]T. Hyakutake and S. Nagai, "Numerical simulation of red blood cell distributions in three-dimensional microvascular bifurcations," Microvasc. Res. **97**, 115–123 (2015).
[15]T. Ishikawa, H. Fujiwara, N. Matsuki, T. Yoshimoto, Y. Imai, H. Ueno, and T. Yamaguchi, "Asymmetry of blood flow and cancer cell adhesion in a microchannel with symmetric bifurcation and confluence," Biomed. Microdevices **13**, 159–167 (2011).
[16]A. Kvon, Y. H. Lee, T. A. Cheema, and C. W. Park, "Development of dual micro-piv system for simultaneous velocity measurements: Optical arrangement techniques and application to blood flow measurements," Meas. Sci. Technol. **25**, 075302 (2014).
[17]L. Lanotte, G. Tomaiulo, C. Misbah, L. Bureau, and S. Guido, "Red blood cell dynamics in polymer brush-coated microcapillaries: A model of endothelial glycocalyx *in vitro*," Biomicrofluidics **8**, 014104 (2014).
[18]X. Li, A. S. Popel, and G. E. Karniadakis, "Blood-plasma separation in Y-shaped bifurcating microfluidic channels: A dissipative particle dynamics simulation study," Phys. Biol. **9**, 026010 (2012).
[19]R. Lima, S. Wada, S. Tanaka, M. Takeda, T. Ishikawa, K. Tsubota, Y. Imai, and T. Yamaguchi, "*In vitro* blood flow in a rectangular PDMS microchannel: Experimental observations using a confocal micro-PIV system," Biomed. Microdevices **10**, 153–167 (2008).
[20]H. H. Lipowsky, S. Usami, S. Chien, and R. R. N. Pittman, "Hematocrit determination in small bore tubes from optical-density measurements under white-light illumination," Microvasc. Res. **20**, 51–70 (1980).
[21]S. Lorthois, F. Cassot, and F. Lauwers, "Simulation study of brain blood flow regulation by intra-cortical arterioles in an anatomically accurate large human vascular network: Part I: Methodology and baseline flow," Neuroimage **54**, 1031–1042 (2011).
[22]S. Lorthois, F. Cassot, and F. Lauwers, "Simulation study of brain blood flow regulation by intra-cortical arterioles in an anatomically accurate large human vascular network. Part II: Flow variations induced by global or localized modifications of arteriolar diameters," Neuroimage **54**, 2840–2853 (2011).
[23]S. Lorthois and F. Lauwers, "Control of brain blood flow by capillaries: A simulation study in an anatomically accurate large human vascular network," Comput. Methods Biomech. Biomed. Eng. **15**(Suppl 1), 66–68 (2012).
[24]S. Lorthois, F. Lauwers, and F. Cassot, "Tortuosity and other vessel attributes for arterioles and venules of the human cerebral cortex," Microvasc. Res. **91**, 99–109 (2014).
[25]K. Lykov, X. Li, H. Lei, I. V. Pivkin, and G. E. Karniadakis, "Inflow/outflow boundary conditions for particle-based blood flow simulations: Application to arterial bifurcations and trees," PLoS Comput. Biol. **11**, e1004410 (2015).
[26]J. McDonald and G. Whitesides, "Poly(dimethylsiloxane) as a material for fabricating microfluidic devices," Acc. Chem. Res. **35**, 491–499 (2002).
[27]D. Obrist, B. Weber, A. Buck, and P. Jenny, "Red blood cell distribution in simplified capillary networks," Philos. Trans. R. Soc., A **368**, 2897–2918 (2010).
[28]T. Patzek and D. Silin, "Shape factor and hydraulic conductance in noncircular capillaries i. One-phase creeping flow," J. Colloid Interface Sci. **236**, 295–304 (2001).
[29]R. Pittman and M. Ellsworth, "Estimation of red-cell flow in microvessels- consequences of the Baker-Wayland spatial averaging model," Microvasc. Res. **32**, 371–388 (1986).
[30]K. Pitts, R. Mehri, C. Mavriplis, and M. Fenech, "Micro-particle image velocimetry measurement of blood flow: Validation and analysis of data pre-processing and processing methods," Meas. Sci. Technol. **23**, 105302 (2012).
[31]C. Poelma, A. Kloosterman, B. P. Hierck, and J. Westerweel, "Accurate blood flow measurements: Are artificial tracers necessary?," PLoS One **7**, e45247 (2012).

[32]A. Pries, G. Kanzow, and P. Gaehtgens, "Microphotometric determination of hematocrit in small vessels," Am. J. Physiol. - Heart Circ. Physiol. **245**, H167–H177 (1983).
[33]A. Pries, B. Reglin, and T. Secomb, "Structural response of microcirculatory networks to changes in demand: Information transfer by shear stress," Am. J. Physiol.: Heart Circ. Physiol. **284**, H2204–H2212 (2003).
[34]A. Pries and T. Secomb, "Microvascular blood viscosity *in vivo* and the endothelial surface layer," Am. J. Physiol.: Heart Circ. Physiol. **289**, H2657–H2664 (2005).
[35]A. Pries, T. Secomb, and P. Gaehtgens, "Biophysical aspects of blood flow in the microvasculature," Cardiovasc. Res. **32**, 654–667 (1996).
[36]A. Pries, T. Secomb, P. Gaehtgens, and J. Gross, "Blood-flow in microvascular networks - Experiments and simulation," Circ. Res. **67**, 826–834 (1990).
[37]A. R. Pries, K. Ley, M. Claassen, and P. Gaehtgens, "Red cell distribution at microvascular bifurcations," Microvasc. Res. **38**, 81–101 (1989).
[38]J. Reichold, M. Stampanoni, A. L. Keller, A. Buck, P. Jenny, and B. Weber, "Vascular graph model to simulate the cerebral blood flow in realistic vascular networks," J. Cereb. Blood Flow Metab. **29**, 1429–1443 (2009).
[39]S. Roman, S. Lorthois, P. Duru, and F. Risso, "An optimized technique for red blood cells velocity measurement in microvessels," J. Biomech. **45**(Suppl 1), S35 (2012).
[40]S. Roman, S. Lorthois, P. Duru, and F. Risso, "Velocimetry of red blood cells in microvessels by the dual-slit method: effect of velocity gradients," Microvasc. Res. **84**, 249–261 (2012).
[41]F. Schmid, J. Reichold, B. Weber, and P. Jenny, "The impact of capillary dilation on the distribution of red blood cells in artificial networks," Am. J. Physiol.: Heart Circ. Physiol. **308**, H733–H742 (2015).
[42]G. Schmid-Schönbein, R. Skalak, S. Usami, and S. Chien, "Cell distribution in capillary networks," Microvasc. Res. **19**, 18–44 (1980).
[43]C. B. Schaffer, B. Friedman, N. Nishimura, L. F. Schroeder, P. S. Tsai, F. F. Ebner, P. D. Lyden, and D. Kleinfeld, "Two-photon imaging of cortical surface microvessels reveals a robust redistribution in blood flow after vascular occlusion," PLoS Biol. **4**(2), e22 (2006).
[44]M. Sharan and A. Popel, "A two-phase model for flow of blood in narrow tubes with increased effective viscosity near the wall," Biorheology **38**, 415–428 (2001).
[45]Z. Shen, G. Coupier, B. Kaoui, B. Polack, J. Harting, C. Misbah, and T. Podgorski, "Inversion of hematocrit partition at microfluidic bifurcations," Microvasc. Res. **105**, 40–46 (2016).
[46]J. M. Sherwood, D. Holmes, E. Kaliviotis, and S. Balabani, "Spatial distributions of red blood cells significantly alter local haemodynamics," PLoS One **9**, e100473 (2014).
[47]J. M. Sherwood, E. Kaliviotis, J. Dusting, and S. Balabani, "Hematocrit, viscosity and velocity distributions of aggregating and non-aggregating blood in a bifurcating microchannel," Biomech. Model. Mechanobiol. **13**, 259–273 (2014).
[48]S. S. Shevkoplyas, S. C. Gifford, T. Yoshida, and M. W. Bitensky, "Prototype of an *in vitro* model of the microcirculation," Microvasc. Res. **65**, 132–136 (2003).
[49]Y. Sugii, R. Okuda, K. Okamoto, and H. Madarame, "Velocity measurement of both red blood cells and plasma of *in vitro* blood flow using high-speed micro piv technique," Meas. Sci. Technol. **16**, 1126–1130 (2005).
[50]A. Villringer, A. Them, U. Lindauer, K. Einhaupl, and U. Dirnagl, "Capillary perfusion of the rat-brain cortex. An *in-vivo* confocal microscopy study," Circ. Res. **75**, 55–62 (1994).